Current Science
Current Science
Current Science
CS 4 (2), 510– 520 (2024)
Received 25 December 2023 | Revised 20 January 2024 | Accepted 25 Februry 2024 | Online Available 20 March 2024
https://doi.org/10.52845/CS/2023-4-2-1

OPEN ACCESS
ISSN(O)2795-8639

ORIGINAL ARTICLE

Preparation and Study of Luminescence Properties of Novel Chalcogenide Niobate Sr_2LaNbO_6:XSm^{3+}

Xianyu Zhang [1], Yingchao Xu [1,2]*, Haoshuang Fan [1], Jing Li [1], Li Li [1], Junhuang Hong [1]

[1]School of Optoelectronics and Communication Engineering, Xiamen University of Technology, Xiamen 361024, China

[2]Fujian Provincial Key Laboratory of Optoelectronic Technology and Devices, Xiamen University of Technology, Xiamen 361024, China

Corresponding Author: Yingchao XU

Abstract

A series of $Sr_2La_{1-x}NbO_6$:xSm^{3+} orange-red phosphors were prepared by a high-temperature solid-phase method, and their physical structure, luminescence properties, fluorescence decay and thermal stability were investigated. It was found that the optimal doping concentration of the samples was x = 0.04, and the concentration burst was mainly attributed to the electric dipole-electric dipole effect. In addition, this orange-red phosphor was not only efficiently excited by near-ultraviolet and blue light to produce orange-red light, the fluorescence lifetime was significantly shortened with the increase of Sm^{3+} doping concentration. In addition, the colour coordinates of all the samples are located in the orange-red region with high colour purity and low associated colour temperature, and these results indicate that the Sm^{3+} doped Sr_2LaNbO_6 orange-red phosphor has a potential application in the field of solid-state lighting.

Key words: Rare earth materials; Sr_2LaNbO_6: Sm^{3+}; High-temperature solid-phase method; White LED; Orange-red phosphor.

Introduction

The market for energy efficient devices is attracting more and more attention, most of today's energy consumption is electricity, which is mainly used in various types of lighting [1-3]. White light-emitting diodes (LED) are considered as the fourth generation of solid state light source after incandescent and fluorescent lamps, which have the advantages of long life, energy efficiency and environmental friendliness [4,5]. The basic method for producing white LEDs is to combine blue LED chips with yellow phosphor (YAG:Ce^{3+}) to produce white light [6]. Currently, the technology of combining blue LED devices with YAG:Ce^{3+} phosphors is well established. However, because of the lack of suitable red phosphors, commercial LED products have large correlated color temperature errors (CTE) and low color rendering index (CRI) [7,8]. Rare earth element ions (e.g., Eu^{2+}、Eu^{3+}、Sm^{3+}和Mn^{4+}) are commonly used as the main additives for red phosphors. Among them, the f-f leaping rare earth ion Sm^{3+} has significant absorption capacity in the UV-visible region. It is widely used as an important material for the production of orange-red phosphors due to the ease with which the electrons in its 4f orbitals can jump from the energy level $^4G_{5/2}$ to ^6H_J (J = 5/2, 7/2, 9/2, 11/2), and this jumping process excites the substrate to emit orange-red light[9-11]. It has been pointed out that Sm^{3+} is able to produce orange-red light in a variety of matrix materials [12-14], such as YPO_4:Sm^{3+}、$La_7Ta_3W_4O_{30}$:Sm^{3+} and $Sr_3La_2GeO_{12}$:Sm^{3+}. In recent years, the research on new red phosphors has attracted much

attention, in which materials such as nitrides and sulfides have been challenged by their high preparation cost and low luminescence efficiency. However, niobate, as an important rare-earth luminescent material, has important applications in the field of materials science. In addition to its wide application in piezoelectric, dielectric and ferroelectric fields, niobate also occupies an important position in rare-earth luminescent materials. In particular, niobates with chalcogenide structure are often used by researchers as substrates for fluorescent materials due to their stable crystal structure and diverse structural species. Composite chalcogenides (e.g., $Ba_3MgNb_2O_9$: Eu^{3+}), dual chalcogenide niobates (e.g., Ba_2GdNbO_6: Sm^{3+} , Ca_2GdNbO_6: Eu^{3+}), and monoclonal chalcogenide niobates (e.g., $NaNbO_3$: Pr^{3+} , $KNbO_3$: Eu^{3+}) are the hot spots of the current research. These materials have a wide range of applications in the field of luminescence, especially the chalcogenide-structured niobate phosphors have attracted much attention due to their diversity.

In this study, a series of Sm^{3+}-doped Sr_2LaNbO_6 phosphors were successfully prepared by a high-temperature solid-phase method, and the structural characterization of the samples, the elemental compositions as well as the optimal concentration of Sm^{3+} doping were investigated, and the photoluminescence performance, thermal stability and fluorescence lifetime of the samples were studied.

2. Experimental methods and procedures

2.1. Sample preparation

In this study, we describe the preparation process of Sr_2LaNbO_6: Sm^{3+} material. Firstly, raw materials including Nb_2O_5（99.9%）、$SrCO_3$（AR）La_2O_3（99.99%）and Sm_2O_3（99.99%）need to be weighed and placed into an agate mortar for thorough grinding. Subsequently, the mixture is placed into an alumina crucible and subjected to high-temperature calcination at 1300°C for 5 hours in a muffle furnace. Following this, the resulting product is naturally cooled to room temperature and appropriately ground to prepare for subsequent performance testing.

2.2. Sample characterization

In this study, we used a PANalytical X'Pert PRO X-ray diffractometer (Panacol, The Netherlands) with Cu Kα radiation, a wavelength (λ) of 0.1541 nm, a working current of 40 mA, and a tube voltage of 40 kV, for powder sample measurements in the scanning range of 20°-70° at a scan speed of 0.02°/sec. The instrument employed a thermal quenching analysis system (Hangzhou Yuanfang Optoelectronic Information Co., Ltd.) and EX-1000 phosphor excitation spectra for color coordinates, temperature-variable spectra, color purity, and color temperature analyses. Additionally, we used the Edinburgh FLS980 steady-state/transient spectrofluorometer to analyze fluorescence lifetimes, emission spectra, and excitation spectra.

3. Results and discussion

3.1. Phase analysis

Figure 1 presents the XRD patterns of $Sr_2La_{1-x}NbO_6$:xSm^{3+}（x=0~0.07）. It is observable from the figure that the major diffraction peaks of Sr_2LaNbO_6 powder doped with Sm^{3+} match the standard JCPDF 47-0461 diffraction peaks. The XRD patterns of samples at different concentrations are essentially consistent, indicating that varying doping concentrations do not alter the phase structure.

The standard Sr_2LaNbO_6 belongs to the tetragonal crystal system, similar to the low-temperature structure with space group Fm3m; the lattice parameters are a=8.260 Å，b=8.260 Å，c=8.246 Å和 V=562.6 $Å^3$. It can be observed from Figure 1 that the XRD pattern is mainly dominated by the Sr_2LaNbO_6 diffraction peaks. However, in Figure 2, additional peaks labeled with ※ corresponding to the Sr_2LaNbO_6 impurities are observed, but their intensity relative to the main diffraction peaks is weak, indicating that the effect of impurities on this study is minimal. As for Sm^{3+} doped Sr_2LaNbO_6 crystals, the ionic radii of cations are: Sr^{2+} =1.18 Å，La^{3+} =1.03 Å，Nb^{5+} =0.64 Å The ionic radius size difference (D_r) between the doping ion (Sm^{3+}=0.96 Å) and the host cations can be estimated using the following formula:

$$D_r = 100\% * \frac{R_m^{(CN)} - R_d^{(CN)}}{R_m^{(CN)}} \quad (1)$$

According to the ion radiation similarity mechanism, $R_m^{(CN)}$and $R_d^{(CN)}$ are the ionic radii of the host and doped cations, given by the *CN*

coordination number. Thus, the D_r values between Eu^{3+} and Sr^{2+} and between La^{3+} and Nb^{5+} can be calculated as 18.6%, 6.8%, and 50%, respectively. Theoretically, the D_r value of the mutually replaceable ions should not exceed 30%; the difference between Sm^{3+} and Sr^{2+} and La^{3+} is small, while the difference between Sm^{3+} and Nb^{5+} far exceeds this limit. Considering the principle of preferential substitution of ions of the same valence state, Sm^{3+} better occupies the La^{3+} site. In this study, we found that Sm^{3+} partially replaces the lattice sites of La^{3+}, while the diffraction peak positions of the doped samples mainly remain unchanged. This indicates that the small amount of Sm^{3+} doping did not significantly alter the crystal structure of Sr_2LaNbO_6.

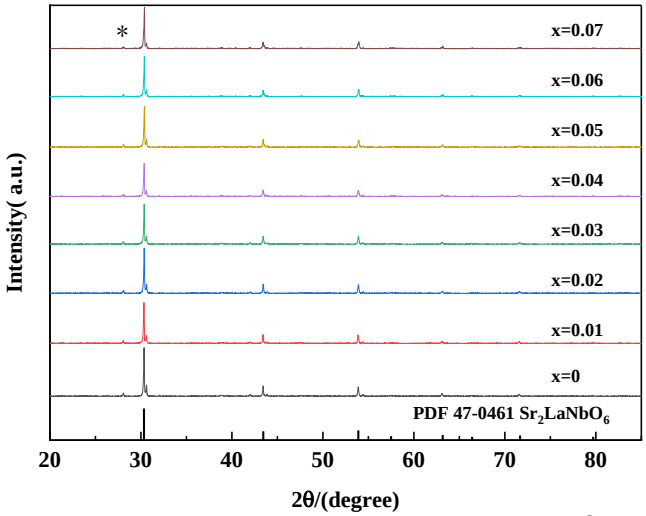

Figure 1 XRD patterns of $Sr_2La_{1-x}NbO_6$:xSm^{3+}

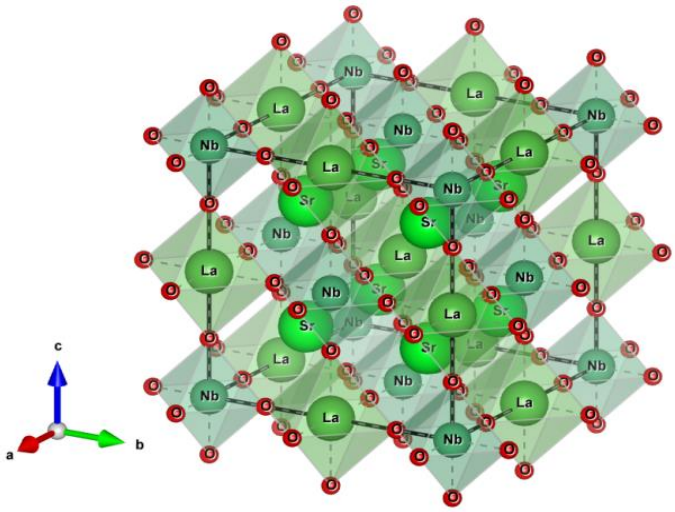

Figure 2 Sr_2LaNbO_6 cell structure

The surface morphology of the optimized doped sample is shown in Figure 3(b), where it can be observed that the majority of the sample has an irregular, smooth surface consisting of granular particles with sizes ranging from 2 to 8 μm. Additionally, there is a small amount of agglomerated larger particles due to the influence of surface energy during high-temperature solid-state synthesis. As the sintering temperature increases, the large grain boundaries expand towards the center of smaller grains, leading to further growth of the larger grains [15].

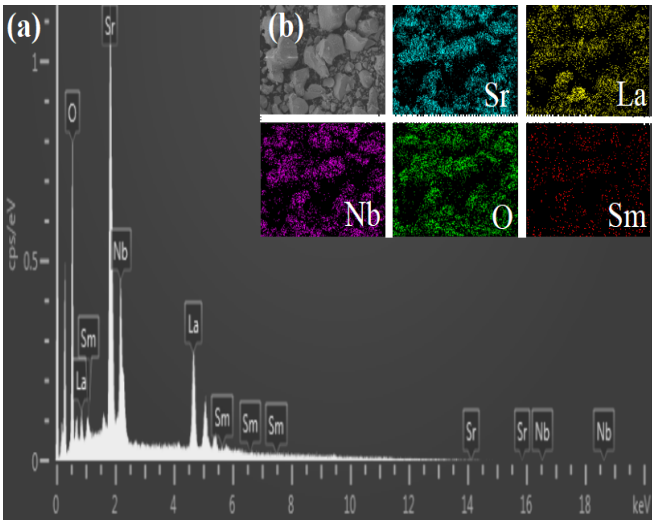

Figure 3 Color distribution and EDS spectra of each element

The elements of the $Sr_2La_{0.96}NbO_6$:0.04Sm^{3+} sample were determined using an energy-dispersive X-ray spectrometer (EDS). Figures 3(a) and (b) show the peak values and the color distribution maps of each element, respectively. From Figures 3(a) and 3(b), it can be observed that the major elements, Sr, La, Nb, O, and Sm, are uniformly distributed throughout the entire sample of phosphor particles. The atomic percentages of the constituents in the matrix are close to the desired ratio of 2:1:1:6, indicating successful incorporation of the Sm^{3+} ions into the lattice of $Sr_2La_{0.96}NbO_6$ through high-temperature solid-state reaction. Furthermore, the EDS spectra exhibit no additional impurity peaks, further confirming the purity of the product.

3.2. Photoinduced spectral analysis

Figure 4 presents the energy level transition diagram of Sm^{3+}, which helps us understand the energy transfer process of Sm^{3+} within the main lattice of Sr_2LaNbO_6:Sm^{3+}. Meanwhile, Figure 5 displays the emission spectrum of $Sr_2La_{0.96}NbO_6$:0.04Sm^{3+} phosphor at a monitoring wavelength of 407 nm (red curve) and the excitation spectrum at a monitoring wavelength of 607 nm (black curve). The excitation spectrum in Figure 5 consists of a series of excitation peaks within the range of 200 to 500 nm; the peak at 275 nm is due to the charge transfer from O_2 to Sm^{3+} (CTB) [16] and the absorption of Sr_2LaNbO_6.

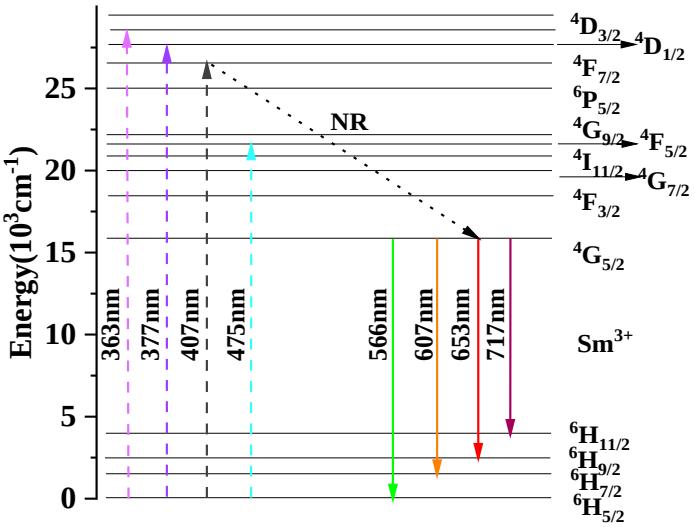

Figure 4 Energy level transition diagram of Sm^{3+}

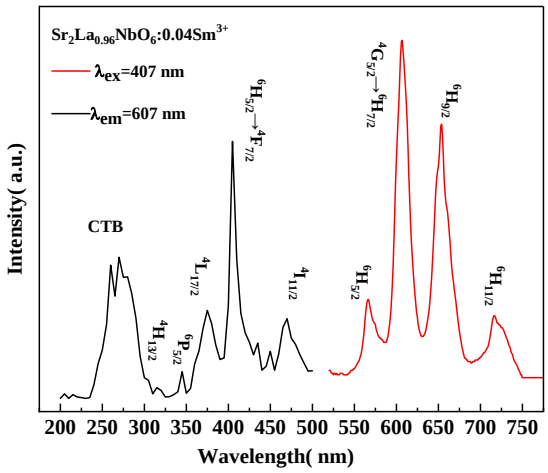

Figure 5 PL excitation and emission spectra of $Sr_2La_{0.96}NbO_6$:0.04Sm^{3+}

Due to the 4f-4f transitions of Sm^{3+}, excitation peaks with different wavelengths are generated, corresponding to different electronic transition pathways of $^6H_{5/2}\rightarrow{}^4H_{13/2}$、$^6H_{5/2}\rightarrow{}^6P_{5/2}$、$^6H_{5/2}\rightarrow{}^4L_{17/2}$、$^6H_{5/2}\rightarrow{}^4F_{7/2}$和$^6H_{5/2}\rightarrow{}^4I_{11/2}$ for the excitation peaks at 348 nm, 363 nm, 363 nm, 407 nm, and 475 nm, respectively [17]. By examining the emission spectrum, it is found that near-ultraviolet LED chips can excite the phosphor and exhibit a wide range of emission wavelengths. Additionally, four characteristic peaks appear in the emission spectrum, corresponding to 567 ($^4G_{5/2}\rightarrow{}^6H_{5/2}$)、607 nm($^4G_{5/2}\rightarrow{}^6H_{7/2}$)、654 nm($^4G_{5/2}\rightarrow{}^6H_{9/2}$) and 717 nm($^4G_{5/2}\rightarrow{}^6H_{11/2}$)[18]. Analysis of the magnetic dipole (MD) and electric dipole (ED) transition rules reveals the lattice symmetry of Sm^{3+}, leading to the conclusion of low network symmetry in its matrix lattice [19,20].

Figure 6(a) displays the emission spectrum of the phosphor $Sr_2La_{1-x}NbO_6$:xSm^{3+}（x=0.01-0.07）, while Figure 6(b) illustrates the relationship between the fluorescence intensity in the 500-750 nm wavelength range and the doping concentration. The crystal structure of the matrix is unaffected by Sm^{3+} doping, hence the shape and position of the emission peaks of $Sr_2La_{1-x}NbO_6$:xSm^{3+} remain unchanged with increasing Sm^{3+} doping concentration, only the intensity varies. The reduced distance between Sm^{3+} ions due to increasing doping concentration leads to energy transfer and consequently results in concentration quenching of the fluorescence in $Sr_2La_{1-x}NbO_6$:xSm^{3+}phosphors. When the Sm^{3+} doping concentration is less than 0.04, the luminescence intensity increases with increasing concentration, reaching its maximum at 0.04. However, above 0.04, the luminescence intensity decreases as the Sm^{3+} doping concentration increases [17]. Concentration quenching is usually associated with energy transfer distance, which can be calculated using formula (2) [21].

$$R_c = 2\left(\frac{3V}{4\pi X_0 N}\right)^{1/3} \qquad (2)$$

Where X_0 is the optimal doping concentration, N is the number of Sr_2LaNbO_6 cations, and V is the crystal cell volume of Sr_2LaNbO_6. For $Sr_2La_{1-x}NbO_6$:xSm^{3+}, X_0=0.04, and thus the calculated critical distance R_c≈23.96Å. When R_c exceeds 5 Å, energy transfer is not the main cause of concentration quenching. The dominant role in concentration quenching effects is played by electric multipole interactions. The numbers 3, 6, 8, and 10 correspond to energy transfer between neighboring ions, dipole-dipole interactions (d-d), dipole-quadrupole interactions (d-q), and quadrupole-quadrupole interactions (q-q) respectively [22].

According to the Dexter theory, the fluorescence intensity I can be obtained using equation (3) [23].

$$\frac{I}{x} = K\left[1+\beta\left(x^{Q/3}\right)\right]^{-1} \qquad (3)$$

The rare earth ion doping concentration is denoted as x, where Q represents the exponent of electric multipole interactions, and K and β are constants under excitation at 407 nm.

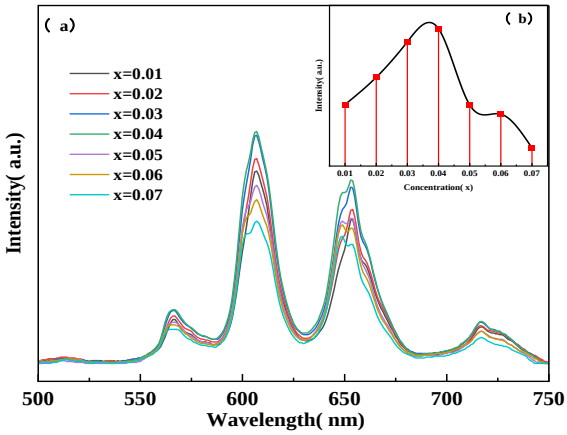

Figure 6 PL spectra of $Sr_2La_{1-x}NbO_6:xSm^{3+}$

(x=0.01~0.07)(a)The dependence of integrated fluorescence intensities of main bands on Sm^{3+} contents(b)

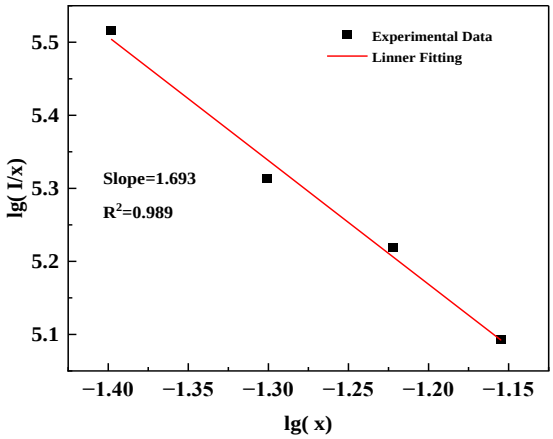

Figure 7 Correlation between lg(*I*/*x*) and lg（*x*）of $Sr_2La_{1-x}NbO_6:xSm^{3+}$ phosphors

Figure 7 illustrates the ratio of log（*I*/*x*） and log（*x*） for the phosphor $Sr_2La_{1-x}NbO_6:xSm^{3+}$（x=0.01-0.07）. The slope of the *Q*/3 curve is approximately 1.69, indicating that the concentration quenching in $Sr_2La_{1-x}NbO_6:xSm^{3+}$ is primarily due to electric dipole-dipole interactions. This suggests that the interaction between ions is of the d-d interaction type.

3.3. The fluorescence attenuation curve was analyzed

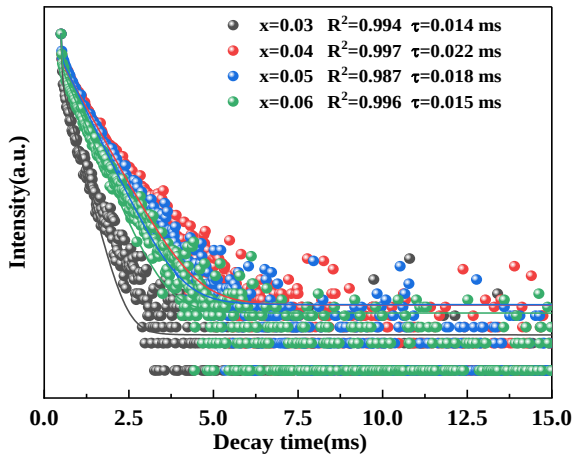

Figure 8 Sm^{3+} emission of $Sr_2La_{1-x}NbO_6:xSm^{3+}$ phosphors excited by 407 nm and monitored at 607 nm

Figure 8 presents the fluorescence decay curve of Sm^{3+} in $Sr_2La_{1-x}NbO_6$:xSm^{3+}(x=0.01~0.07) at 607 nm, which is excited at 407 nm.The time decay curve of the luminescence intensity exhibits a single exponential function nature, and is fitted by the following equation (4):

$$y = A_1 \exp\left(-\frac{x}{t}\right) + y_0 \qquad (4)$$

In the above context, y represents the luminescence intensity corresponding to x, A_1 is a constant, t is the decay time, and y_0 is the luminescence intensity at time 0. The black curve represents the exponential decay curve, and the fitted data indicates that the fluorescence lifetime of the sample $Sr_2La_{0.96}NbO_6$:0.04Sm^{3+} is 0.022 ms. With the increase of Sm^{3+} concentration, the fluorescence lifetime of the sample gradually decreases. The main reason for this is the reduction in the distance between Sm^{3+} ions, leading to increased interactions, increased self-absorption rate of Sm^{3+}, and an increased probability of non-radiative transitions [24].

3.4. Variable temperature spectrum and thermal stability analysis

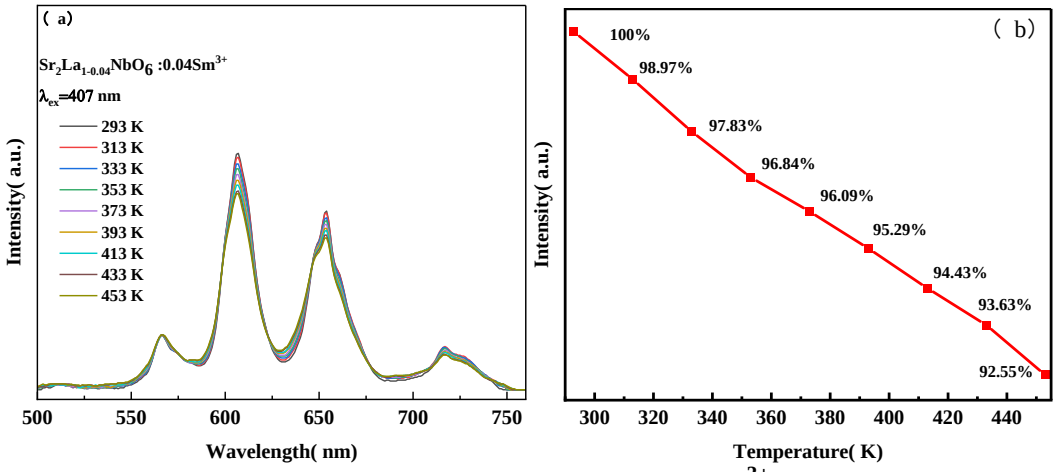

Figure 9 Comparison of emission spectra of $Sr_2La_{0.96}NbO_6$:0.04Sm^{3+} and the fluorescence intensity of samples at different temperatures upon excitation of 407 nm(b)

Figure 9(a) shows the emission spectra of $Sr_2La_{0.96}NbO_6$:0.04Sm^{3+} phosphor excited at 407 nm under different temperatures. As observed in Figure 9(b), at a temperature of 453 K, the luminescence intensity can still maintain 92.55% of the room temperature fluorescence intensity. In comparison to other studies, at 423 K, the luminescence intensity of Ca_2LaNbO_6: Sm^{3+} was 65.26% of the room temperature intensity [25], at 406 K, the luminescence intensity of YPO_4: Sm^{3+} was 87.6% of the room temperature intensity [26], and at 453K, the luminescence intensity of Ca_2GdNbO_6: Sm^{3+} was 65.32% of the room temperature intensity [27]. This indicates that compared to other similar types of phosphors, Sr_2LaNbO_6: xSm^{3+} orange-red phosphor exhibits better thermal stability.

The activation energy E_a for thermal quenching of Sm^{3+}-doped Sr_2LaNbO_6 phosphor can be calculated using formula (5) [28].

$$\ln\left(\frac{I_0}{I} - 1\right) = \ln(A) - \frac{E_a}{K_B T} \qquad (5)$$

T represents the temperature, K_B is the Boltzmann constant (8.62×10-5 eV), A is a constant, I is the fluorescence intensity at a specific temperature, and I_o is the fluorescence intensity at room temperature.

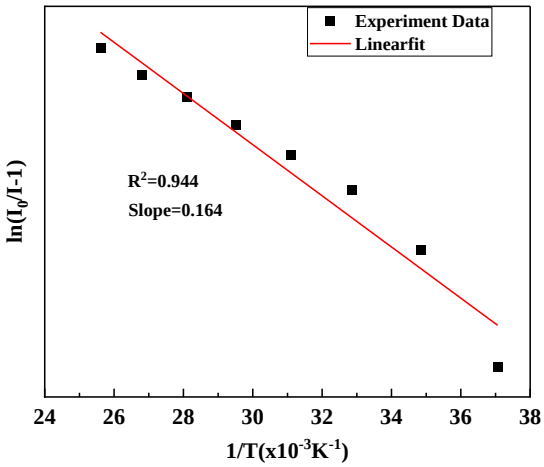

Figure 10 Plot of ln(I_0/I-1) versus 1/K_BT for $Sr_2La_{0.96}NbO_6$:0.04Sm^{3+} samples

Figure 10 illustrates the relationship between the fluorescence *ln（I_0/I-1）* and *1/K_BT* for $Sr_2La_{0.96}NbO_6$:0.04Sm^{3+} phosphor. The slope obtained from the linear fit is -0.16. According to equation (5) calculation, the E_a value is determined to be 0.16 eV, which is higher than other similar phosphors. These results demonstrate that $Sr_2La_{0.96}NbO_6$:0.04Sm^{3+} exhibits excellent thermal stability, indicating their potential for enhanced application in WLEDs.

3.5. Sample color coordinate

Table 1 lists the color purity, chromaticity coordinates, and correlated color temperature data for $Sr_2La_{1-x}NbO_6$:xSm^{3+} samples. The observations indicate that all samples exhibit high color purity, which is crucial for the emission performance of LEDs. Furthermore, the observed low correlated color temperature has the potential to address the issue of high correlated color temperature in traditional white LEDs and provides ideal color performance for the application of LED light sources.

Figure 11 displays the CIE chromaticity coordinates for $Sr_2La_{1-x}NbO_6$:xSm^{3+} samples. The emission chromaticity coordinates of different concentrations are all located in the orange-red region, indicating that the phosphor exhibits excellent orange-red emission performance and holds potential for applications in the field of white LEDs.

Table.1 The colour coordinates, correlated colour temperature and colour purity of phosphors $Sr_2La_{1-x}NbO_6$:*x*Sm^{3+}

Sm^{3+}浓度	色坐标	色纯度	相关色温/K	相对亮度
0.01	（0.6174，0.38）	99.4	1289	3588
0.02	（0.6155，0.3818）	99.3	1302	3983
0.03	（0.6188，0.3795）	99.6	1278	4467
0.04	（0.6212，0.3775）	99.8	1260	4626
0.05	（0.6243，0.3748）	99.9	1236	3594
0.06	（0.6187，0.3793）	99.5	1280	3467
0.07	（0.6202，0.3785）	99.8	1267	3081

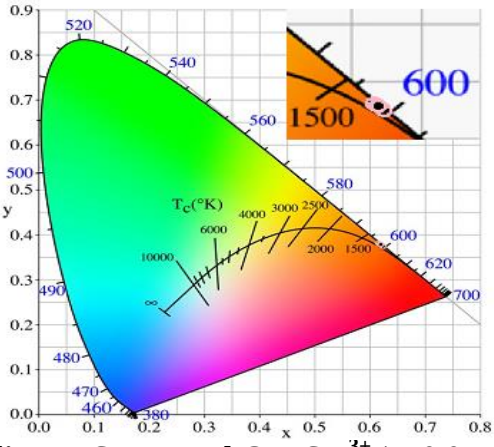

Figure 11 CIE coordinates $Sr_2La_{1-x}NbO_6:xSm^{3+}$ (*x*=0.01~0.07) coordinates

4. Conclusions

A series of $Sr_2La_{1-x}NbO_6:xSm^{3+}$（x=0~0.07）phosphor materials were prepared through high-temperature solid-state synthesis. Under excitation at 407 nm, Sm^{3+} emitted intense orange-red light at 607 nm. The concentration quenching in the samples was found to be due to dipole-dipole interactions, as indicated by theoretical analysis. Increasing the doping concentration of Sm^{3+} resulted in a decrease in interionic distances. This phenomenon led to an increase in nonradiative transition probability, thereby reducing the fluorescence lifetime of the samples. For $Sr_2La_{1-x}NbO_6:xSm^{3+}$ samples, no significant decrease in luminescence intensity was observed even at high temperatures (453 K), maintaining a level of 92.55% compared to room temperature. Furthermore, the samples exhibited low color temperature and high color purity. Based on these characteristics, $Sr_2LaNbO_6:xSm^{3+}$ phosphors have significant potential for application in the field of white LED lighting.

Acknowledgements

This work was supported by The University Industry-University-Research Joint Innovation Proiect of Fujian Province (No.2023H6038).

Author contributions

XYZ: conceptualization, investigation, experiment, writing–original draft. YCX: methodology, data curation, supervision. HSF: formal analysis, writing–review and editing. JL: investigation, experiment. LL: investigation, experiment. JHH: investigation, experiment. All authors read and approved the final manuscript

Data availability

All data generated or analyzed during this study are included in this paper

Declarations

Conflict of interest The authors declare that they have no known competing financial interests or personal relationships that could have appeared to influence the work reported in this paper

Reference

1. Jun Huang. Preparation and luminescence properties of rare earth doped phosphors such as phosphate, tungstate and niobate [D]. Guangdong: Guangdong University of Technology,2015.DOI:10.7666/d.Y2796301.（in Chinese）
2. F Li, Yin-Yin Tang, Shi-xiu Cao, et al. Effect of Eu^{3+} doping concentration on luminescence characteristics of $Gd_{6-x}WO_{12}:xEu^{3+}$ red phosphor [J]. China Lighting Electric Appliances,2019(1):1-5.（in Chinese）DOI: 10.3969/j.issn.10026150.2019.01.001.（in Chinese）
3. X X Hu. Study on synthesis and luminescence properties of rare Earth doped niobate phosphor [D]. Guangdong University of Technology, 2018.（in Chinese）
4. Lanchi Xie, Xin Luo, Weibin Yang, et al. Preparation and Luminescence Properties of Sm^{3+} doped Sr_2YSbO_6 Red Phosphor [J]. New chemical materials, 2022,50(9):84-88.（in Chinese）
5. Jing Wang, Jitao LU, Mingjun SONG Mingjun. Preparation and luminescence properties of Sm^{3+} ion activated $Ba_3ZnNb_2O_9$ phosphor [J]. Guangzhou Chemical, 2022,

50(12):65-67. （in Chinese）DOI:10.3969/j.issn.10019677.2022.12.019. （in Chinese）
6. Zhenya Li, Xue-Yan Chen, Fangfang HU, et al. Preparation, Structure and Fluorescence Properties of $Ca_2Y_8(SiO_4)_6O_2:Eu^{3+}$ phosphor [J]. Chinese Journal of rare Earth, 2019,37(5):530-536. DOI:10.11785/S1000-4343.20190502. （in Chinese）
7. Shaohua,Tian Zheng Qiao, Mingsheng Sun. Luminescence and Energy Transfer of Color-adjustable phosphors $Ca_9Al(PO_4)_7:Tb^{3+}$, Sm^{3+}used in White LEDs [J]. Chinese Journal of Luminescence, 2019, 40(12): 1469-1477. （in Chinese）
8. Wang S, Han Y jie, Shi L, 等. A novel single-phased $Sr_4La_6(SiO_4)_6Cl_2:Dy^{3+}$ phosphor for white-light-emitting diodes[J]. Inorganic Chemistry Communications, 2020,117:107948.
9. Leiming Zheng, Ming Wang, Si Chen, et al. Research progress of single substrate phosphor excited by near ultraviolet [J]. Chinese Journal of Chemical Engineering, 2021,72(7):3551-3561. DOI:10.11949/0438-1157.20201795. （in Chinese）
10. Zhao Li, Jing Cao, Yongfeng Wang, et al. Preparation and photoluminescence of $NaGd(WO_4)_2$:Sm^{3+} phosphor [J]. Rare earth,2021,42(2):25-29. DOI:10.16533/J.CNKI.15-1099/TF.20210020. （in Chinese）
11. Lu Wang. Study on preparation and Luminescence properties of Red phosphor for white LED [D]. Inner Mongolia: Inner Mongolia University,2020. （in Chinese）
12. Caiwen Shi, Changyan Ji, Ting Zeng, Zeng Ting, et al. Synthesis and properties of High color purity and high thermal stability red phosphor $Sr_3La_2Ge_3O_{12}:Sm^{3+}$ [J]. Journal of Inorganic Chemistry, 2020,36(5):901-907. DOI:10.11862/CJIC.2020.112. （in Chinese）
13. Wang X, Li Y X, Li J, Yu G L, Zuo L, Huang H W. Microwave dielectric properties and applications of $Ba(Zn_{1/3}Nb_{2/3})O_3Ca(Zn_{1/3}Nb_{2/3})O_3$ composite ceramics by one-step synthesis method[J]. Journal of Materials Science: Materials in Electronics, 2014,25(11): 4720-4724.[N].
14. Wu J X, Li M, Jia H L, Liu Z G, Jia H , Wang Z Z. Morphology formation mechanism and fluorescence properties of nano-phosphor YPO:Sm^{3+}excited by near-ultraviolet light J[J]. l. J. Alloys Compd., 2019, 821:153535.
15. Shuang Wang, Yajie Han, Lei Shi, et al. Synthesis of Y_2WO_6:Sm^{3+} red phosphor by high temperature solid phase method [J]. Journal of Hebei Normal University of Science and Technology,2019,33(4):60-65. DOI:10.3969/J.ISSN.1672-7983.2019.04.010. （in Chinese）
16. Ouertani G, Ferhi M, Horchani-Naifer K, Ferid M. Effect of Sm^{3+}concentration and excitation wavelength on spectroscopic properties of $GdPO_4:Sm^{3+}$phosphorJj.[J]. (J. Alloys Compd, 2021, 885:161 178.).
17. Xianguo Meng, Qiong Zhou, Yingchao Xu, et al. Study on photoluminescence properties of novel Orange-red phosphor $Sr_4Nb_2O_9$: Sm^{3+} [J]. Chinese Journal of rare Earth, 2023,41(2):272-278. DOI:10.11785/S1000-4343.20230207. （in Chinese）
18. Panpan Wu, Xianguo Meng, Yingchao Xu, et al. Novel orange-red phosphor doped with Sm^{3+} $NaSr_2Nb_5O_{15}$ [J]. Laser journal,2022,43(8):37-42. DOI:10.14016/j.cnki.jgzz.2022.08.037.（in Chinese）
19. Qingjun Zhang, Huangqing Liu, Lingling Wang. Synthesis and properties of $La_2O_3:Sm^{3+}$ nanoluminescent materials by combustion method [J]. Rare metal materials and engineering,2019,48(1):133-136. （in Chinese）
20. Jinyan Li, Qimin DENG, Dejian HOU. Study on luminescence properties of Sm^{3+} ion doped $Sr_2P_2O_7$ materials [J]. Guangdong Chemical Industry,2020,47(13):14-15,30. DOI:10.3969/j.issn.1007-1865.2020.13.008. （in Chinese）
21. Zhang x, Cui R R, Zhang J, Yuan G F, Qi X S, Deng C Y. Structural and photoluminescence properties of a novel $Ba_2GdNbO_6:Sm^{3+}$ phosphor [Jl.Optics,2021:167646[J].
22. Yong,Zhang FH Xu, Xyi TANG, et al. Synthesis and photoluminescence properties of high color purity Ca_3La_7 $(SiO_4)_5(PO_4)O_2:Sm^{3+}$ phosphor [J]. Journal of Huaiyin Normal University (Natural Science Edition), 2019,18(3):222-227. （in Chinese）
23. Fan J, Zhang W, Dai S, et al. Effect of charge compensators A^+ (A = Li, Na and K) on luminescence enhancement of $Ca_3Sr_3(PO_4)_4$:

Sm^{3+} orange-red phosphors[J]. Ceramics International, 2018, 44(16): 20028-20033.
24. Miaomiao Tian, Panlai Li, Zhijun Wang, et al. Synthesis, color-tunable emission, thermal stability, luminescence and energy transfer of Sm^{3+} and Eu^{3+} single-doped $M_3Tb(BO_3)_3$ (M = Sr and Ba) phosphors[J]. CrystEngComm, 2016, 18(36): 6934-6947.[N].
25. Zunhua Li, Yongbiao Hua, Guangchuan Ou. Synthesis red-emitting Ca_2LaNbO_6:xSm^{3+} phosphors for good color-rendering-index white-LED[J]. devices[J]. Optik, 2021,233:1 66595.
26. Aleksandar Ćirić, Stevan Stojadinović, Milica Sekulić, et al. JOES: An application software for Judd-Ofelt analysis from Eu^{3+} emission spectra[J]. Journal of Luminescence, 2019,2 05: 351-356.[J].
27. Yongbin Hua, Jae Su Yu. Synthesis and luminescence properties of reddish-orange-emitting Ca_2GdNbO_6:Sm^{3+} phosphors with good thermal stability for high CRI white applications[J]. Ceramics International, 2021, 47(5): 6059-6067.
28. Gao Z, Xue N, Jeong JH, 等. $SrBi_2TeO_7$:Eu^{3+}: A novel blue-light excitable red-emitting phosphor for solid-state lighting[J]. Materials Research Bulletin, 2017, 95: 497-502.